

# Generation of Short Intense Terahertz Pulses Through Optical Rectification

Carl Ekström

Diploma Project  
Supervisor: *Jörgen Larsson*  
LRAP 510



**LUND**  
UNIVERSITY

### **Abstract**

The lack of sources that generates intense THz pulses have in many years limited the field of THz science. Until recently intense THz pulses have been hard to generate using nonlinear crystals such as Lithium Niobate (LiNbO<sub>3</sub>) with high efficiency. In this thesis a method is presented for achieving short and intense THz pulses through optical rectification using the recently developed tilted pulsefront technique. This method involves using an amplified pulsed Ti:Sapphire laser and a LiNbO<sub>3</sub> crystal. The thesis describes the theory behind THz generation and the practical steps required in order to implement it. The final design is portable and has a high conversion efficiency of 0.08% and intense THz pulses with energies up to 0.4  $\mu$ J were generated.

# Contents

<b>Contents</b>	<b>3</b>
<b>1 Acknowledgments</b>	<b>5</b>
<b>2 Outline</b>	<b>5</b>
<b>3 Introduction</b>	<b>6</b>
3.1 Introduction to THz science . . . . .	6
3.1.1 Applications . . . . .	7
3.2 The aim of the project . . . . .	7
<b>4 Theory</b>	<b>9</b>
4.1 Single-cycle THz pulses through optical rectification . . . . .	9
4.1.1 Nonlinear polarization density . . . . .	9
4.1.2 OR from difference frequency generation . . . . .	9
4.1.3 The source of radiation . . . . .	10
4.2 Phase and velocity matching in LiNbO <sub>3</sub> -crystal . . . . .	11
4.2.1 Collinear and noncollinear THz generation in LiNbO <sub>3</sub> . . . . .	11
4.2.2 Group and phase index for LiNbO <sub>3</sub> . . . . .	12
4.2.3 Wave mixing coherence length . . . . .	14
4.2.4 Doping and absorption . . . . .	15
4.2.5 Tilting the pulsefront using a grating . . . . .	16
<b>5 Theoretical calculations and results</b>	<b>18</b>
5.1 Group and phase-index calculations . . . . .	18
5.1.1 Tilt-angle in crystal . . . . .	18
5.2 Imaging of the grating in LiNbO <sub>3</sub> crystal . . . . .	18
5.2.1 Optimal magnification for the lens system . . . . .	19
5.3 Generated frequencies . . . . .	21
5.4 Crystal geometry . . . . .	22
5.5 Setup design . . . . .	23
<b>6 Method</b>	<b>25</b>
6.1 Building of the setup . . . . .	25
6.1.1 Tilting . . . . .	25
6.2 Detection of THz radiation . . . . .	26
6.3 Improvements of the setup . . . . .	26
6.3.1 Adjusting the crystal . . . . .	26
6.3.2 Mirror replacement . . . . .	26
6.3.3 Spectral cut from lens . . . . .	27
6.3.4 The amplified Ti:Sapphire laser . . . . .	27
6.3.5 Increased intensity with a telescope . . . . .	27
6.3.6 Final setup . . . . .	28
6.4 Final measurements . . . . .	29

<b>7</b>	<b>Experimental results</b>	<b>30</b>
<b>8</b>	<b>Discussion of results and conclusions</b>	<b>35</b>
8.1	Detection and power . . . . .	35
8.2	Spatial profile . . . . .	35
8.3	Polarization . . . . .	37
8.4	Telescope . . . . .	37
<b>9</b>	<b>Summation of the project</b>	<b>37</b>
<b>10</b>	<b>Appendix</b>	<b>38</b>
10.1	Measuring power with Pyroelectric THz detector . . . . .	38
10.2	Imaging with NEC THz camera . . . . .	39
10.2.1	Spatial filter and frame integration . . . . .	39
10.3	Sellmeier equation for LiNbO <sub>3</sub> . . . . .	41
10.4	The Gaussian beam . . . . .	42
10.5	Equipment used in the project . . . . .	43
	<b>References</b>	<b>44</b>

## 1 Acknowledgments

I would like to thank my supervisor Jörgen Larsson for giving me this opportunity to do this project on my own and supervising me in the right direction when I was confused. I would also thank Henrik Enquist for spending lot of time when the laser equipment broke down from time to time as well as inspiring discussions about the project.

Finally I also want to thank all people in the Ultrafast X-ray science group at the division of Atomic Physics and MAX IV laboratory for good advices as well as ordering optical components or just by interesting discussions.

Special thanks goes to Carlito Ponseca at Chemical Physics for letting me borrow his THz detector when our detectors malfunctioned.

## 2 Outline

This thesis consists of 6 main parts. First in section 3 there will be an introduction to THz science and why this spectral range is interesting. Some of the possible applications will be discussed as well as the aim of this project. Two theory parts, one describing the general theory and the other the theoretical methods and calculations that leads to the optical design is presented in section 4 and 5 respectively. The practical work of the project is then presented in section 6. The experimental results is then presented in section 7 and finally discussed in section 8. In the discussion part of the thesis the conclusions about the project is also stated.

### 3 Introduction

#### 3.1 Introduction to THz science

THz radiation can be described as electromagnetic radiation spanning the frequency gap between the mid infra-red and microwave frequencies in the middle of the two main areas of electronics and photonics. This is often defined to be between 0.1-10 THz [1] and is illustrated in figure 1.

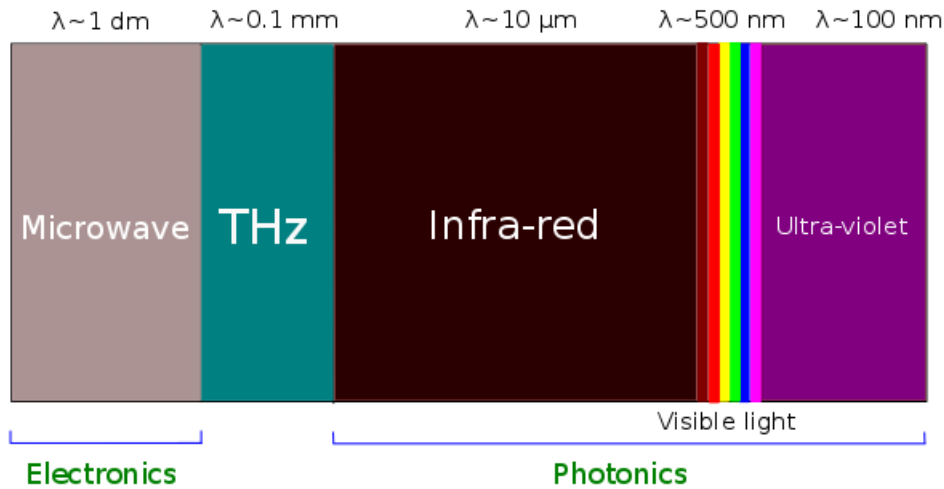


Figure 1: The electromagnetic spectrum

The radiation in this range has been of interest for applications for the military as well as airports and other industries for several years [2]. The research has been more intensified the last two decades due to the development of generation methods that are more portable and can establish pulses with high intensities. The lack of high energy THz sources and good detectors have been called the *THz-gap*.

One reason for the growing interest in THz science are that the radiation is safe for non-invasive investigations since the photons have considerable less energy than the photons of x-ray radiation but easily penetrates many common materials like textile, plastic and paper [1].

The previous generation of a pulsed THz radiation source was the photoconductive (PC) switch [3], (see figure 2). The PC switch can also be used to detect THz radiation. A PC switch emits a THz pulse when the area between two biased electrodes are hit by an ultrashort laser pulse. That is due to the acceleration of created charges in that area. This method of a PC switch could unfortunately only generate low energy pulses due to limitations such as absorption in the substrate.

Another way to achieve THz pulses was through optical rectification (OR) using materials with high nonlinear response to ultrashort laser pulses. This

project is based on a recently developed OR technique in a LiNbO<sub>3</sub> crystal.

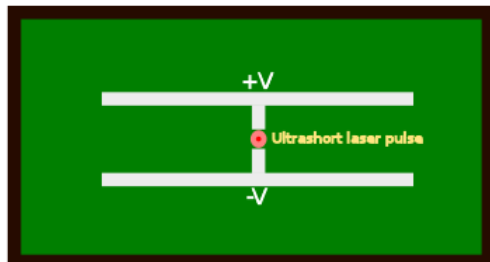


Figure 2: A photo-conductive antenna switch for emitting THz radiation.

To achieve really high energies one could also use free electron lasers [2]. This generation method has the disadvantage of non-practical use outside research areas as well as size and costs of the equipment.

The detectors used earlier in the 1990s was often the PC switch as mentioned or based on some kind of Electro-optic sampling [2]. But in recent years pyroelectric detectors specialized for THz detection has been developed making it easier and cheaper to detect the radiation calibrated at room temperatures. Together with the new OR technique it is now possible to build a portable setup that can generate intense broadband THz pulses with good efficiency and measure the power at room temperatures.

Palm-sized THz cameras are now also available on the market which makes THz alignment as well as detection and profile imaging much easier.

### 3.1.1 Applications

A lot of molecules shows response to THz radiation because many of these compounds have their vibrational and rotational modes in this frequency range [2]. Consequently the THz research- and engineering area has gained more attention in developing practical techniques that make use of it, like detecting explosives or drugs. A novel application in research is to image structural dynamics in materials. Since the THz band consists of sub-mm wavelengths the resolution is also better compared to microwave imaging.

A particularly good example of practical use is to detect explosives with THz spectroscopy. Many of the commonly used explosives have distinct absorption lines in the THz spectrum (see table 1 in [2]).

Another example of a practical use is to detect weapons. Figure 3<sup>1</sup> shows detection of a knife with THz imaging.

## 3.2 The aim of the project

The aim of this diploma project is to see how one can generate short and intense THz pulses using the tilted pulse front technique [4]. This includes building a

<sup>1</sup>Image from <http://thznetwork.net/index.php/thz-images>



Figure 3: Detection of a knife with THz radiation.

portable setup, measuring the efficiency, using a THz camera to measure the profile of the beam and optimize the setup. The project was done at the MAX IV laboratory in Lund and at the division of Atomic Physics, Lund University.



## 4 Theory

In this section, the physics behind the OR process will be explained as well as how one can achieve THz radiation through OR in a LiNbO3 crystal using the tilted pulsefront. In section 4.1 the theory behind THz pulse generation through OR in general is presented and in section 4.2 specifically how this efficiently can be achieved in LiNbO3.

### 4.1 Single-cycle THz pulses through optical rectification

In electronics rectification is when you rectify your signal from alternating current (AC) to direct current (DC). In a nonlinear crystal a varying optical electric field can analogously induce a so called DC polarization density in the crystal [5]. To describe this, one have to go to the basic theory of second order nonlinear optics. The polarization density as well as the electric field is described by vectors but scalar equations will be used here to easily understand the principle.

#### 4.1.1 Nonlinear polarization density

In a linear dielectric medium the polarization density and the optical electric field have the linear relation:

$$P = \epsilon_0 \chi E \quad (1)$$

where  $\epsilon_0, \chi$  and  $E$  is the permittivity in vacuum, susceptibility and electric field respectively. This means that in a linear material the induced dipole moments responds proportional to the electric field. For a nonlinear material exposed to a high electric field this can instead be described by a Taylor expansion of the induced polarization density describing higher order susceptibilities  $\chi^{(n)}$ . Induced *second order* nonlinear polarization density, which occurs in materials which lack inversion symmetry, can then be described by the second term of this expansion as [5]:

$$P_{NL}(t) = \frac{1}{4} \epsilon_0 \chi^{(2)} E(t)^2 = 2dE(t)^2 \quad (2)$$

where  $\chi^{(2)}, d$  and  $E(t)$  is the second order nonlinear susceptibility, nonlinear coefficient and the optical electric field respectively.

#### 4.1.2 OR from difference frequency generation

If it is assumed that the optical field consists of two frequency components,  $\omega_1$  and  $\omega_2$ , the field can be described as:

$$E(t) = E_1 \cos(\omega_1 t) + E_2 \cos(\omega_2 t) \quad (3)$$

Substituting this optical field in equation 2 gives that the nonlinear polarization density will be a sum of five different components at five frequencies,  $0, 2\omega_1, 2\omega_2, \omega_1 + \omega_2$  and  $\omega_1 - \omega_2$  [5]. One of them, as seen, will describe an

induced polarization density at the difference frequency. The component that describe this is:

$$P_{NL-}(t) = \frac{1}{4}\epsilon_0\chi^{(2)}E_1E_2\cos((\omega_1 - \omega_2)t) = dE_1E_2\cos((\omega_1 - \omega_2)t) \quad (4)$$

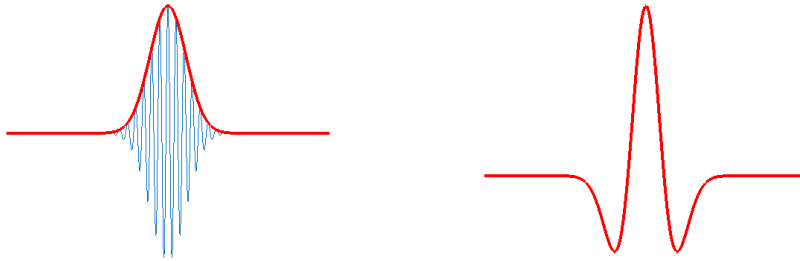
This process is basically the method of THz generation through OR. What this means is that generation of THz frequencies can be seen as difference frequency generation with all the spectral components in a laser pulse. Using an ultrashort Ti:Sapphire laser with broad spectral range and central wavelength around 800nm gives difference frequencies in the THz range [3]. The total polarization density that contributes to the THz generation will then be the sum of all the polarization densities induced by equation 4. If it is assumed that the laser pulse is Gaussian shaped with a slowly varying envelope compared to the period times of the spectral components the sum of all induced polarization densities will then have the Gaussian shape of that envelope [1].

#### 4.1.3 The source of radiation

From the nonlinear wave equation [5] it is shown that the second time derivative of a nonlinear polarization density can be treated as a source of electromagnetic radiation in the crystal. This gives consequently that:

$$E(t)_{THz} \propto \frac{\partial^2 P_-(t)}{\partial t^2} \quad (5)$$

where  $P_-(t)$  is the sum of induced polarization densities from the difference frequency generation. The principle is illustrated in figure 4.



(a) Optical pulse (blue) induces a polarization density with gaussian shape (red)

(b) Generated THz-pulse from the polarization density

Figure 4: The principle of pulsed OR generating a THz pulse

## 4.2 Phase and velocity matching in LiNbO3-crystal

### 4.2.1 Collinear and noncollinear THz generation in LiNbO3

THz generation through OR can be achieved in many nonlinear crystals. One commonly used crystal is Zinc Telluride (ZnTe). In this project a LiNbO3 crystal will be used. LiNbO3 has the advantage of a significantly larger effective nonlinear coefficient  $d_{eff}$  than many other crystals used for OR [3]. As seen in equation 2 a higher coefficient increases the generation efficiency.

The group- and refractive indexes in all materials varies depending on frequency due to dispersion. This is also important to consider when a laser pulse and the generated THz pulse propagates in the same crystal.

The use of ZnTe crystals for THz generation has the advantage that the group index of a laser pulse centered at 800nm and the refractive index at THz frequencies are almost equal [4]. This means that all generated THz in the crystal will sum up in phase as the laser pulse propagates in the crystal resulting in efficient single-cycle THz generation. This is called *collinear* velocity matching.

The LiNbO3 crystal has, compared to ZnTe, a significant difference in the group- and refractive indexes which makes the generation efficiency low for collinear velocity matching. By letting a small optical laser pulse propagate in the crystal and using Huygens principle one can see that all the THz sources (blue circles) will only be in phase forming a THz pulsefront at two directions, each with an angle  $\gamma$  relative to the laser pulse velocity. The difference between the laser pulse propagating in ZnTe and LiNbO3 is illustrated in figure 5.

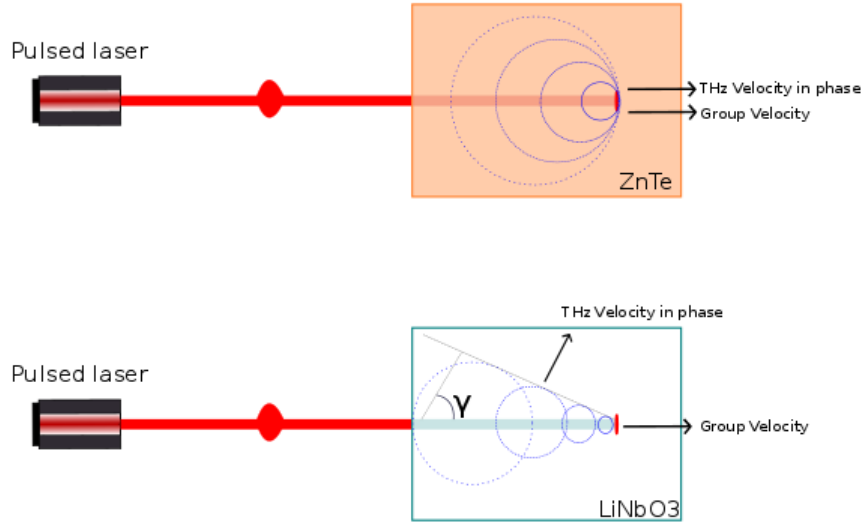


Figure 5: The difference between THz generation in ZnTe and LiNbO3. The blue circles represent the THz sources.

Figure 5 shows a simplified generation that assumes only one source at each propagation time rather than a plane pulsefront which would be a line of sources out of phase with each other. To be able to sum up the generated THz radiation in phase one can then simply tilt the laser pulsefront at the angle  $\gamma$  which makes that all THz sources will be in phase and sum up to an intense single-cycle THz pulse. This is illustrated in figure 6 and is called *noncollinear* velocity matching.

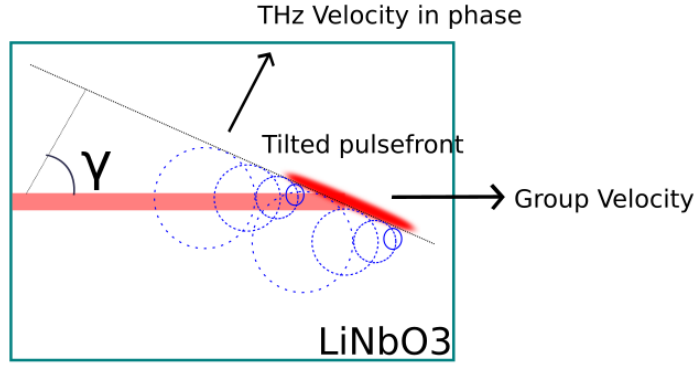


Figure 6: The tilted pulsefront gives efficient THz generation at one certain direction.

The tilt angle  $\gamma$  can then be calculated from the magnitude of the velocity vectors to be:

$$\gamma = \arccos\left(\frac{v_{THz}}{v_{gr}}\right) = \arccos\left(\frac{n_{gr}}{n_{THz}}\right) \quad (6)$$

#### 4.2.2 Group and phase index for LiNbO3

An optical pulse traveling in the crystal will experience the group index [5]:

$$n_{gr} = n - \lambda_0 \frac{dn}{d\lambda_0} \quad (7)$$

where  $n$ ,  $\lambda_0$  and  $dn/d\lambda_0$  are the refractive index, central wavelength and the refractive index change respectively.

Depending of the polarization and direction of the pulse relative to the optic axis of the crystal the refractive index in equation 7 can be calculated from the Sellmeier equations which is found in appendix 10.3.

For the generated THz pulse the phase index can approximately be determined from a polynomial fitted from measurements done by Pálfalvi et al. [6]:

$$n_{thz}(\nu_w) = A + B\nu_w^2 + C\nu_w^4 \quad (8)$$

where  $\nu_w$  is the frequency wavenumber in  $\text{cm}^{-1}$  and  $A, B, C$  are polynomial coefficients found in the mentioned article.

For stoichiometric LiNbO<sub>3</sub> doped with 0.68% mol Mg at room temperature the phase index for frequencies between 0.3-4.5 THz with polarization parallel to the optic axis is shown in figure 7. This is the type of crystal that will be used.

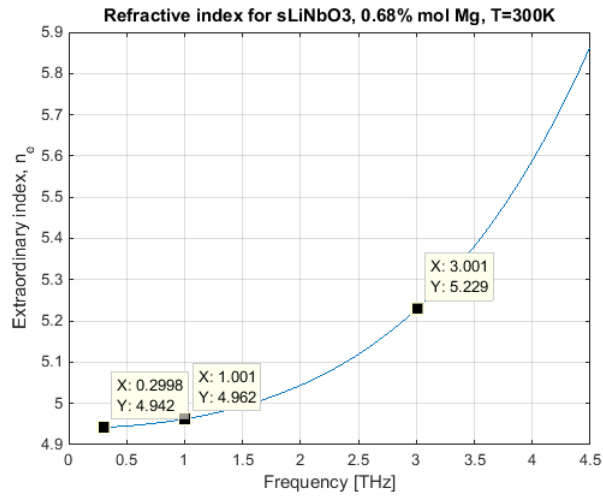


Figure 7: Phase index for stoichiometric Mg-doped LiNbO<sub>3</sub> at room temperature with some values for 0.3, 1 and 3 THz

### 4.2.3 Wave mixing coherence length

To be able to get some understanding about which THz frequencies  $\Omega$  that will be generated it can be good to look at the wave mixing coherence length which is the length in the crystal where the generated THz frequencies sum up coherently and contribute to the THz spectrum. This coherence length is defined by [5]:

$$L_c = \frac{2\pi}{|\Delta k|} \quad (9)$$

where  $\Delta k = k(\omega) + k(\Omega) - k(\omega + \Omega)$  which approximately is:

$$\Delta k \approx k(\Omega) - \Omega \frac{dk}{d\omega} = \Omega \frac{n_{thz}(\Omega)}{c_0} - \Omega \frac{d}{d\omega} \left( \omega \frac{n_{gr}}{c_0} \right) = \frac{\Omega}{c_0} (n_{thz}(\Omega) - n_{gr}) \quad (10)$$

if it is assumed that  $\Omega \ll \omega_0$ , where  $\omega_0$  is the central angular frequency of the optical pump pulse and  $\Omega$  is the THz angular frequency.

Since the matching is a noncollinear case with the pulsefront tilted the propagation is  $1/\cos \gamma$  times longer [7] for the pump pulse which gives the equation:

$$\Delta k \approx \frac{\Omega}{c_0} \left( n_{thz}(\Omega) - \frac{n_{gr}}{\cos \gamma} \right) \quad (11)$$

This gives then that the wave mixing coherence length for the tilted pulsefront will be:

$$L_c(\Omega) = \frac{2\pi c_0}{\left| \Omega \left( n_{thz}(\Omega) - \frac{n_{gr}}{\cos \gamma} \right) \right|} \quad (12)$$

#### 4.2.4 Doping and absorption

The optical damage resistance in the crystal can be improved by doping the LiNbO3 crystal with Mg [11]. It has been found that a concentration of 0.6% mol Mg is good and this is the concentration of Mg in the crystal used in this project.

LiNbO3 shows also like many other materials absorption. From measurement done by Pálfalvi et al. [6] the absorption coefficient for THz radiation in LiNbO3 similar with doping level near the one used in this project has been determined for some THz frequencies, shown in figure 8.

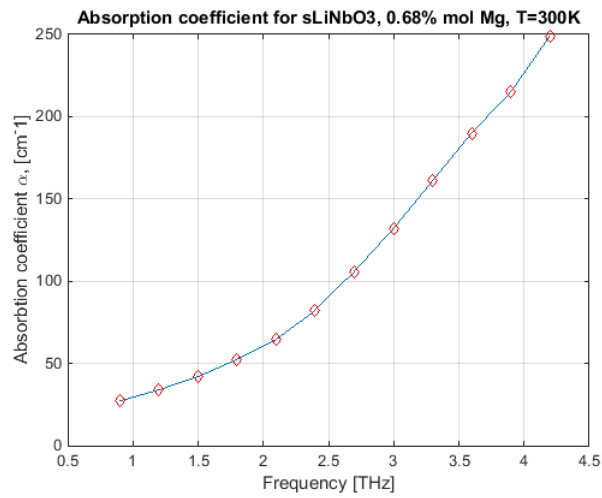


Figure 8: Measured absorption coefficient

#### 4.2.5 Tilting the pulsefront using a grating

As seen previously the pulsefront has to be tilted. The tilting of the pulsefront can be introduced with a reflection grating and a lens system with a certain magnification [8].

The grating equation for first order diffraction is:

$$\sin \theta_i = \frac{\lambda}{d} - \sin \theta_d \quad (13)$$

where  $\theta_i$  is the incident angle,  $\lambda$  is the central wavelength of the pulse,  $d$  the distance between the slits and  $\theta_d$  the diffraction angle.

The incoming pulsefront with an angle  $\theta_i$  relative to the normal will be diffracted and have the outgoing angle  $\theta_d$  according to equation 13 at the interference maximum.

In a simple sketch, such as the one shown in figure 9 it can be seen that the requirement of constructive interference dictates that the second ray of the incoming pulsefront has to travel a distance  $x + y$  longer than the first one. The pulsefront tilt can be calculated from the fact that the difference is a wavelength ( $x + y = \lambda$ ). Both rays will then still have a pulsefront in phase but the front will now be tilted.

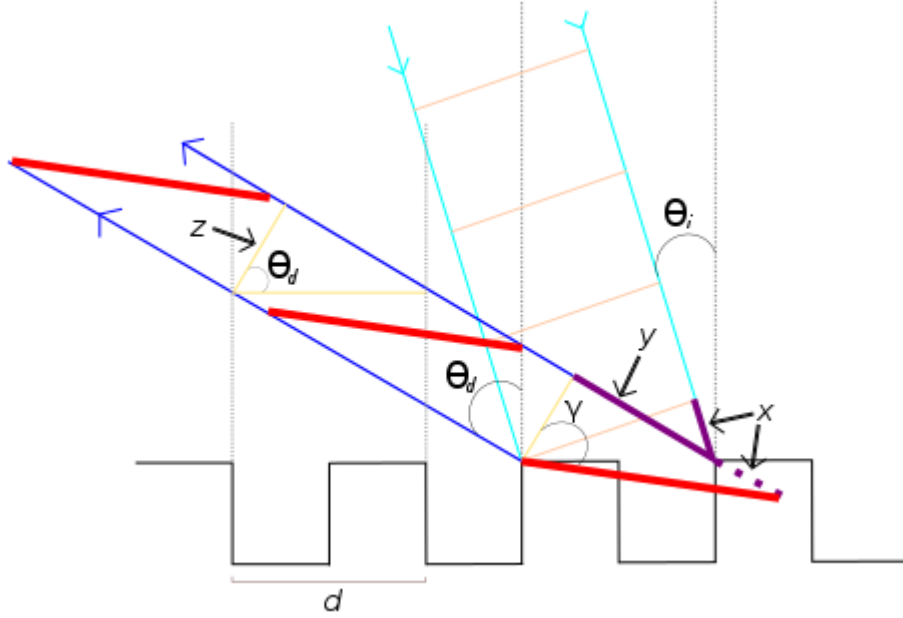


Figure 9: Tilting the pulsefront with a grating. The bold red line represents the tilted pulsefront with tilting angle  $\gamma$

It can be seen that  $z = d \cos \theta_d$  and the tilting angle  $\gamma$  can then be determined by:



$$\tan \gamma = \frac{x + y}{z} = \frac{\lambda}{d \cos \theta_d} \quad (14)$$

In figure 9  $\gamma$  is now the tilted pulsefront *outside* the crystal. To actually calculate the tilt angle of the pulsefront inside the crystal the dependence of the group index in the crystal must be taken to account. It is also required to introduce a horizontal magnification factor  $\beta_m$  since a lens system with some magnification has to be used to collimate and then focus the horizontal tilt inside the crystal. The magnification factor can simply be described as:

$$z_m = \beta_m z \quad (15)$$

where  $z$  and  $z_m$  are the distance before and after magnification respectively.

Substituting  $\lambda = \lambda_0/n_{gr}$  and  $z_m$  instead of  $z$  in equation 14 gives the tilt angle inside the crystal:

$$\tan \gamma = \frac{\lambda_0}{n_{gr} z_m} = \frac{\lambda_0}{n_{gr} \beta_m d \cos \theta_d} \quad (16)$$

## 5 Theoretical calculations and results

In this section calculations leading to the design of the setup are given. If nothing else is stated then:

- The central wavelength of the optical pump pulse will always be  $\lambda_0 = 790nm$ .
- The THz frequency will be 1 THz.
- The number of grooves/mm for a grating is  $1800mm^{-1}$ .

### 5.1 Group and phase-index calculations

From figure 7 it can be seen that for a frequency of 1 THz the phase index will be around  $n_{thz} = 4.962$ .

To determine the group index  $n_{gr}$ , the orientation of the polarization of the propagating optical pulse relative to the optic axis of the crystal must be taken in to account.

Since the nonlinear coefficient for polarization parallel to the optic axis  $d_{33}$  in LiNbO3 is largest it is advantageous to let the optical pulse propagate with a polarization parallel to the optic axis to benefit from larger induced polarization density. The pulse will then experience the extraordinary refractive index  $n_e$  of the crystal according to the index ellipsoid [5]. The extraordinary index is calculated from the Sellmeier equation for LiNbO3 to be  $n_e = 2.176$  for  $\lambda_0 = 790nm$ . The Sellmeier equation is given in appendix 10.3.

From equation 7 the group index can now be determined to be:

$$n_{gr} = n_e - \lambda_0 \frac{dn_e}{d\lambda_0} = 2.176 - 0.79\mu m \cdot (-0.115\mu m^{-1}) \approx 2.267 \quad (17)$$

with  $dn_e/d\lambda_0 = -0.115\mu m^{-1}$  found in the appendix.

#### 5.1.1 Tilt-angle in crystal

As known from section 4.2 the tilt angle inside the LiNbO3 crystal can be calculated from equation 6 which gives that the optimum tilt angle inside the crystal is:

$$\gamma = \arccos\left(\frac{n_{gr}}{n_{THz}}\right) = \arccos\left(\frac{2.267}{4.962}\right) = 62.8^\circ \quad (18)$$

### 5.2 Imaging of the grating in LiNbO3 crystal

The tilt is introduced by the grating but will be further increased using a lens system [8]. The lens system also image the grating inside the crystal. The image of the grating inside the crystal through a lens system with magnification  $\beta$  can be described by [9]:

$$\tan \theta = n_{gr} \beta \tan \theta_d \quad (19)$$

where  $\theta$ ,  $n_{gr}$ ,  $\beta$  and  $\theta_d$  are the grating angle in the crystal, group index, magnification of the imaging lens system and the diffraction angle from the grating respectively. The principle is shown in figure 10.

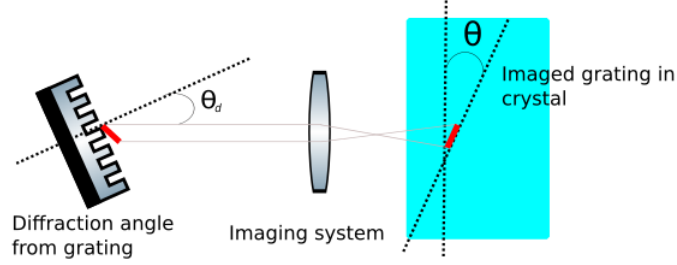


Figure 10: The principle of imaging the grating in the crystal with a lens system.

### 5.2.1 Optimal magnification for the lens system

According to Fülöp et al. [7] the most efficient generation of THz in the crystal will be achieved when the pump pulse duration is shortest. For the tilted pulse, this is at a minimum directly after the diffraction grating or at an image of this point. What this means practically is that the best generation is achieved if the image of the grating and the tilted pulsefront coincides in the crystal, i.e by substituting  $\theta = \gamma$  in equation 19.

By knowing this and using the earlier calculated values the equations 19 and 16 can be rewritten as magnification functions depending on the diffraction angle  $\theta_d$ .

$$\beta_m = \frac{\lambda_0}{n_{gr} d \cos \theta_d \tan \gamma} \quad (20)$$

$$\beta = \frac{\tan \gamma}{n_{gr} \tan \theta_d} \quad (21)$$

By plotting both functions in the same figure for some values of  $\theta_d$ , seen in figure 11, an intersection point can be found where the magnifications are equal (shown by Hirori et al. in [9]).

As seen in figure 11 magnification and diffraction angle should be:

$$\beta = \beta_m = 0.58 \quad (22)$$

$$\theta_d = 56^\circ \quad (23)$$

Now knowing  $\theta_d$  gives that the incident angle on the grating  $\theta_i$  can be calculated from equation 13 and should be:

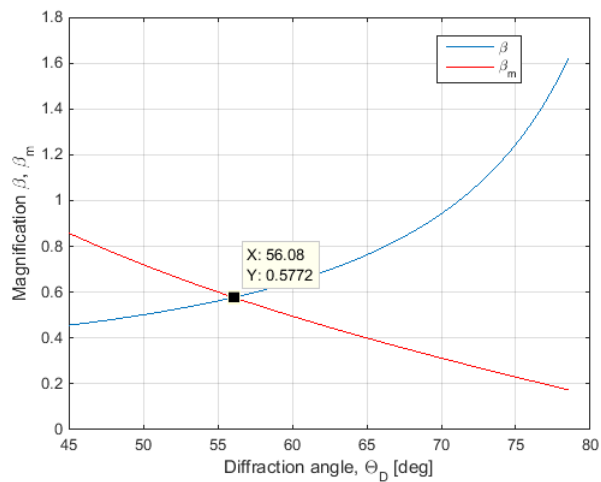


Figure 11: Magnifications as functions of the diffraction angle  $\theta_d$

$$\theta_i = \arcsin\left(\frac{\lambda}{d} - \sin \theta_d\right) = \arcsin\left(\frac{790nm}{10^{-3}m/1800} - \sin 56^\circ\right) = 36.4^\circ \quad (24)$$

### 5.3 Generated frequencies

Since the tilt angle is calculated one can theoretically assume that if the pulse is properly tilted and there is no absorption the spectrum generated could be described by the wave mixing coherence length. Using equation 12 and equation 8 one can calculate the theoretical wave mixing coherence length. The coherence length for tilt angle  $\gamma = 62.8^\circ$  is shown in figure 12 for 0.5-3 THz.

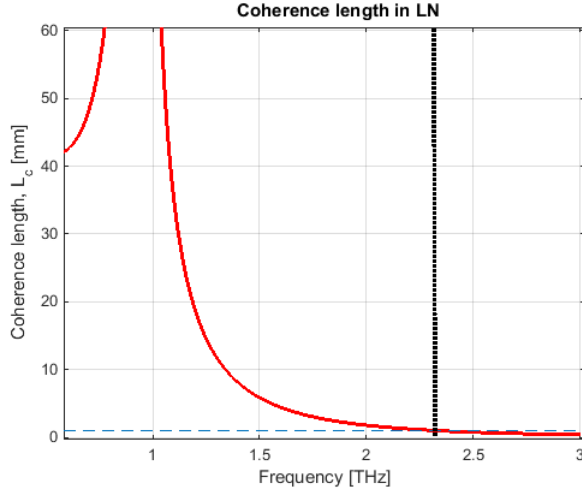


Figure 12: Coherence length for  $62.8^\circ$  tilted angle in LiNbO<sub>3</sub>. The blue dotted line shows where the coherence length is 1 mm which is around 2.3 THz.

Comparing with simulations of generated THz frequencies done earlier in LiNbO<sub>3</sub> with the tilted pulsefront (e.g in [7]) shows that this can be a rough model describing which frequencies that in general will be generated. That is due to the fact that considerably less amount of frequencies over 3 THz seems to not be generated. The generated frequencies depends obviously of the spectral bandwidth of the laser pulse. But as shown above even higher THz frequencies generated from broader laser pulses also have a significantly shorter coherence length which will make the lower part of the THz spectrum dominant independently of the spectral bandwidth of the laser.

## 5.4 Crystal geometry

The calculations of the tilt-angle  $\gamma$  inside the crystal and knowing the orientation of polarization at the entrance of the crystal gives that a reasonable design for the LiNbO<sub>3</sub> crystal can be made. The realized design is shown in figure 13.

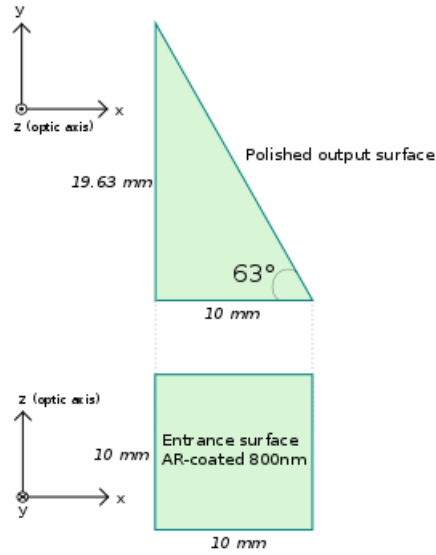


Figure 13: Geometry of the LiNbO<sub>3</sub> crystal.

The crystal is doped with 0.6% mol Mg, have a polished THz output surface and an anti-reflective coating for 800nm on the entrance surface.

In figure 14 the principle is shown when the optical pump pulsefront enters the crystal. The angle  $\gamma^*$  represents the tilt outside the crystal.

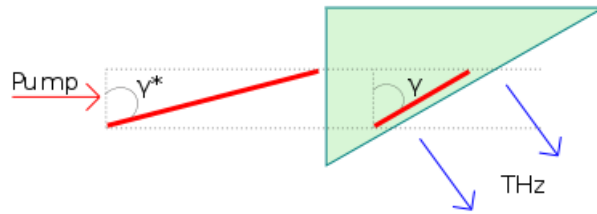


Figure 14: Principle of the tilted wavefront entering the crystal.

## 5.5 Setup design

From previous calculations and investigations, the design for a possible setup can be carried out. The setup has to be portable and is therefore designed to fit a 60x30 cm<sup>2</sup> optical breadboard. The design is shown in figures 15-16.

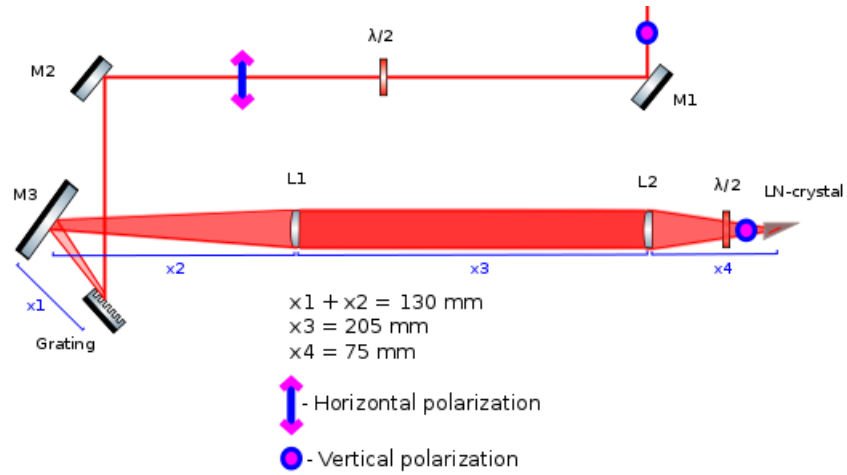


Figure 15: The principle of the tilted pulse-front setup

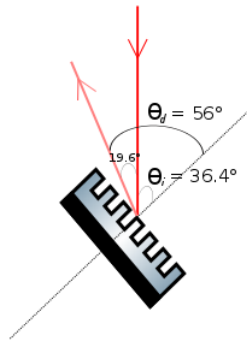


Figure 16: Close view of the grating with the calculated angles.

The pump pulse with vertical polarization will enter the setup. A half-wave plate change the polarization before the grating because the diffraction from the grating is more efficient for this polarization. The pulse then hits the grating which introduces angular dispersion and the now tilted optical pulse reflects on a mirror and then collimated and focused through a 4f cylindrical lens-system with  $f_1 = 130\text{mm}$  and  $f_2 = 75\text{mm}$ . The lens-system gives a horizontal magnification of  $\beta_m = f_2/f_1 = 0.58$  which corresponds to the optimal calculated value of equation 22.

After passing through the lenses the polarization changes back to vertical and the pulse is finally focused in the LiNbO<sub>3</sub> crystal which will emit a THz pulse at the output surface.



## 6 Method

In this section the method of how the setup was built will first be presented and after that how the measurements were done. The equipment used can be found in appendix 10.5.

### 6.1 Building of the setup

The first step to realize the setup was to check that every component physically could be mounted on the optical breadboard as in figure 15. The grating was quite bulky but all the optical components could be mounted on the breadboard.

The lenses were mounted on translation stages to be able to facilitate adjustments of the distances  $x_1$  to  $x_4$ . The grating and the crystal were both mounted on rotational stages so that fine adjustments of the tilt angle and phase-matching could be done.

The height of the laser beam was set to be at the height of around 140mm from the breadboard surface in order to avoid changing the laser beam height and all optical components were adjusted to this height. The alignment of the beam through the optical components were then done with a diode laser and some irises to get the beam as straight as possible. Since the diode laser was continuous and at another wavelength than the pump laser the alignment from the grating to the crystal could not be done properly through the lenses. The alignment for this distance was done with the Ti:Sapphire laser. However to get a rough but good image of the grating on the crystal position a piece of white paper with a barcode pattern was taped carefully on the grating surface. The paper was then illuminated by white light and the lenses was adjusted until the barcode pattern was observable at the crystal position.

#### 6.1.1 Tilting

Since the grading on the rotational stage of the grating was at an unknown offset one had to be able to get a rough measurement of the incident angle on the grating in another way. In figure 16 the angle between the incident and the diffracted beam is  $19.6^\circ$ . The solution was to cut two triangles of cardboard, one with an apex angle  $19^\circ$  and another with  $22^\circ$ . One could then adjust so the incident and the diffracted path of the beam was roughly between the two types of triangles. Since the size of the beam after the grating diverges due to angular dispersion, the diffracted beam was measured from the middle of the observable spot. To validate that this method was good enough the 0:th order of the grating was also used to verify that the path of the beam seemed to be good.

When the adjustment of the grating was done, the mirror  $M3$  was adjusted to reflect the beam from the grating through the lenses. The  $\lambda/2$ -plates was also mounted. Finally the 0:th diffraction order from the grating was blocked.

## 6.2 Detection of THz radiation

After verifying that the beam was going through the setup, the LiNbO<sub>3</sub> crystal was mounted so that the beam had normal incidence on the entrance surface as illustrated in figure 14.

The amplified Ti:Sapphire laser were then used to get the first results. Power measurements was made using a pyroelectric THz detector from Microtech instruments which was connected to an oscilloscope. This detector was used together with an optical chopper from Thorlabs that chopped the pump laser. The chopper was set to 10Hz chopping frequency which according to the data sheet is the frequency that has a responsivity of around 1800V/W at 1 THz. The detector was also mounted on an XYZ translation stage to be able to do the measurement as good as possible.

To avoid measuring the power from the pump laser, the detector has a black filter that blocks the near infrared radiation.

After some adjustments, mainly of the grating and the mirror *M3* the oscilloscope showed the first detected radiation. The peak-to-peak amplitude of the voltage shown on the oscilloscope was noted and was then converted to power according to the responsivity of the detector. To be able to see if the power actually came from THz radiation some tests was done. First the  $\lambda/2$ -plate before the crystal was rotated so that the polarization of the beam entering the crystal was changed. After that a single and a double Si-wafer was mounted after the crystal as a filter blocking the pump laser light to observe the transmittance of the THz radiation at normal incidence. The THz camera was also used to actually see a spot on a screen. Finally a THz polarizer was used to investigate the polarization of the emitted radiation.

## 6.3 Improvements of the setup

### 6.3.1 Adjusting the crystal

Higher efficiency was achieved when the crystal was realigned. The optical beam was adjusted so that the beam entering the crystal was around 1-2mm to the right on the entrance surface relative to the center. Further on the image of the optical pulse inside the crystal was aligned back and forth about max 5mm. Longer distances made the measured THz power drop rapidly. The highest efficiency was given when the image was estimated to be close to the exiting surface, at approximately 0-1.5 mm distance.

### 6.3.2 Mirror replacement

The mirror *M3* of size 1" was too small for the tilted beam after the grating so it was replaced by a 2" mirror. One other advantage of changing this mirror was that any adjustment of the grating would affect the beam on the mirror which in the case of a small one would be more difficult to adjust properly.

### 6.3.3 Spectral cut from lens

One could also observe that the lens  $L1$  was too small in the horizontal direction which cut the spectral width of the beam as seen in figure 17. The width of this lens was 25mm.

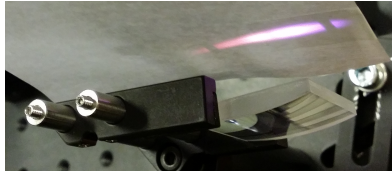


Figure 17: The spectral cut of the beam after the first lens  $L1$ .

$L1$  was then replaced with a similar lens but with twice the width (50mm).

### 6.3.4 The amplified Ti:Sapphire laser

The amplified Ti:Sapphire laser cavity was also adjusted. Since the laser pulse goes through several optical components it is affected from dispersion effects like group velocity dispersion (GVD) that broadening the pulse. By precompensating the stretcher in the amplifier one could compensate for GVD introduced by the components in the setup so that the pulse when entering the crystal is optimal for achieving high generation efficiency.

### 6.3.5 Increased intensity with a telescope

Cylindrical lenses was used to introduce demagnification in the vertical direction of the pulse through a simple Galilean telescope to be able to increase the intensity. The principle is shown in figure 18 and was mounted before the setup.

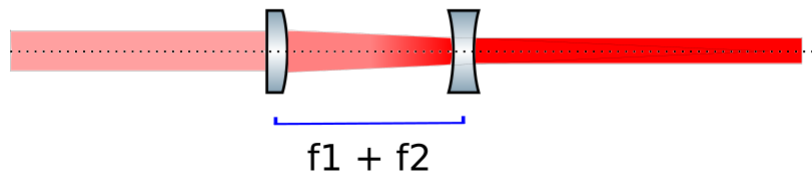


Figure 18: The telescope used for demagnification.

The three different telescopes used had vertical demagnification with a factor of  $M_D = 1.2, 1.6, 2$ . Telescope designs with greater demagnification could be constructed but were not used because of the risk of damaging the crystal.

### 6.3.6 Final setup

The final setup is shown in figure 19 and figure 20 as a sketch and a photograph. Figure 20 b) showing a close view of the crystal.

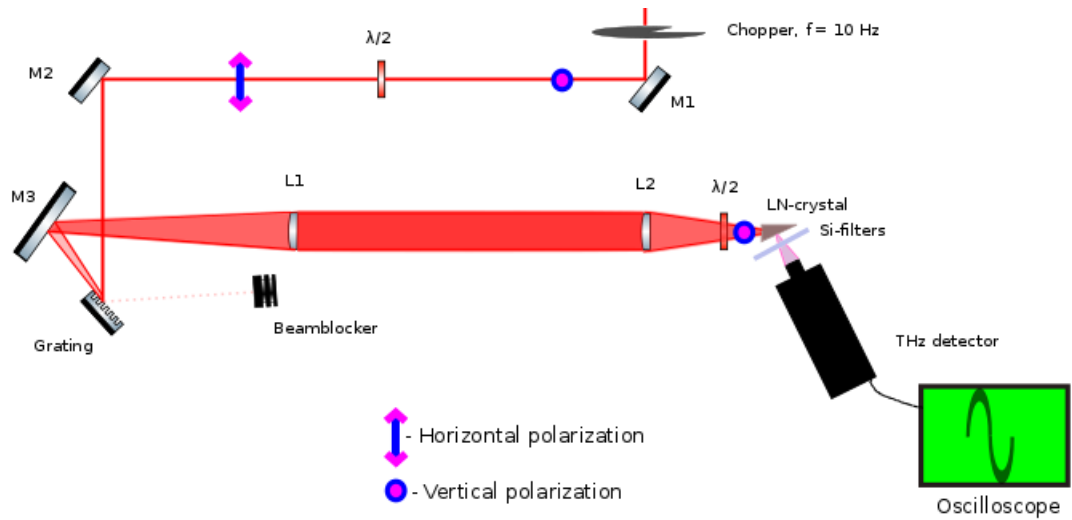
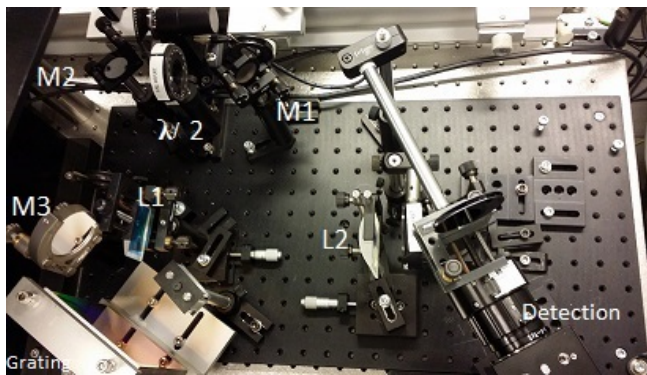
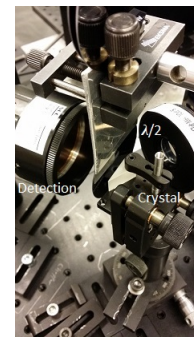


Figure 19: The final setup for detecting THz radiation.



(a) Photo of final setup



(b) Close view of crystal

Figure 20: Photo of the setup

## 6.4 Final measurements

After optimization, the power measurements were made at different input powers, and with alternating one or two Si-filters before the detector. The power of the emitted THz radiation was measured with the different telescope designs as well as without any telescope. Alternating two Si-filters made it possible to calculate the power transmittance of a filter and from that determine the actual THz power leaving the crystal without the risk of burning the detector or measure any optical power.

The grating reflected some of the incoming power at the 0:th diffraction order. This power was measured to give the percentage loss of the power entering the crystal and was subtracted from the input power.

The source in the crystal was captured with the THz camera. The focus ring was carefully adjusted so that the spot was as good as possible. The focus was determined to be good when it could be seen that a piece of cardboard attenuated a part of the beam and not only decreased the intensity. From the captured image the size and profile of the THz spot could be determined as well as the intensity of the THz source. The beam profile was also captured from different distances of the output surface by letting the beam hit on the camera chip directly.

A measurement of the THz power was also done with another pyroelectric power meter, i.e not for THz measurements, and with an ordinary power meter. This was done with one Si-wafer to block the optical frequencies.

## 7 Experimental results

### Spot size and the first measurements

The size of the spot from the pump laser was measured to be approximately 6mm in diameter when entering the setup and the focused spot size at the crystal distance could approximately be determined to be an ellipse with major radius 3mm and minor radius of 1.6mm.

Using the camera the first detected THz spot is shown in figure 21. This image was only captured for detection.

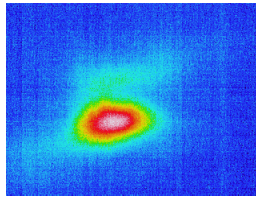


Figure 21: Image of the first THz spot.

The spectral loss due to the first used lens L1 is shown in figure 22.

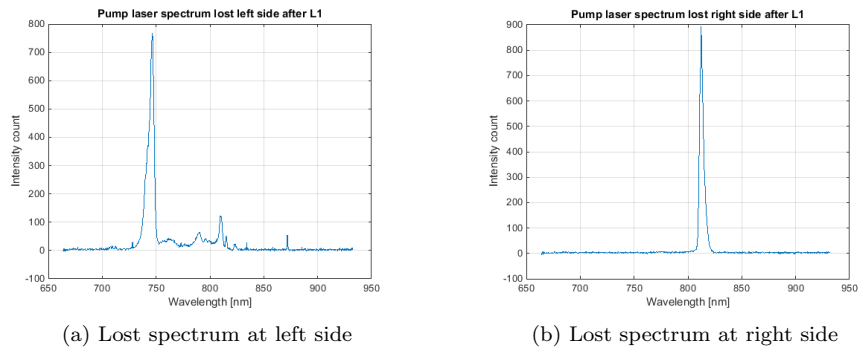


Figure 22: Lost spectrum after the first used lens L1.

### Power and efficiency

After the major improvements the measured pulse energy and conversion efficiency can be seen in figure 23 for different telescope designs. The reflected percentage loss from the grating are subtracted from the values and was measured to be at average 6.2% of the incoming power.

The power measured by the other pyroelectric detector and one Si-filter was determined to be 1.34mW at 2.35W input power.

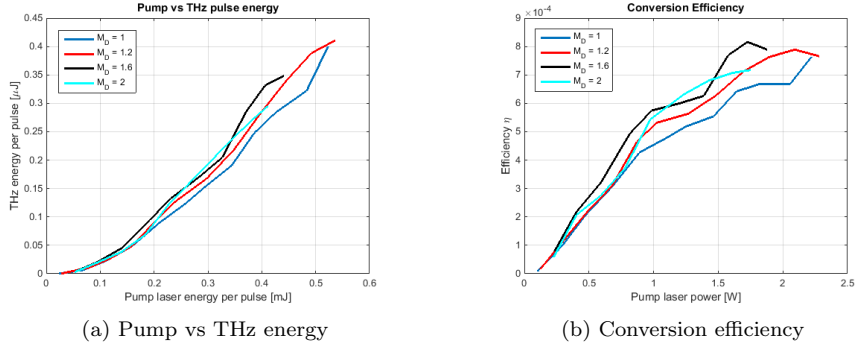


Figure 23: Measured pulse energy and conversion efficiency for different telescope designs with demagnification  $M_D$

### Polarization and power transmittance

Using the THz polarizer the polarization of the emitted radiation could be determined to be almost vertical. In figure 24 b) the voltage as a function of the angle of the polarizer is shown together with the theoretical behaviour of a polarizer. At  $0^\circ$  the wire grid of the polarizer was vertically aligned, i.e parallel to the polarization of the laser.

The measured power transmittance for one Si-wafer that was used to calculate the actual THz power is shown in figure 24 a) and seemed to be close to the theoretical transmittance for normal incidence, which can be calculated from the Fresnel equation (found in [5]) and using the refractive index at THz frequencies [10].

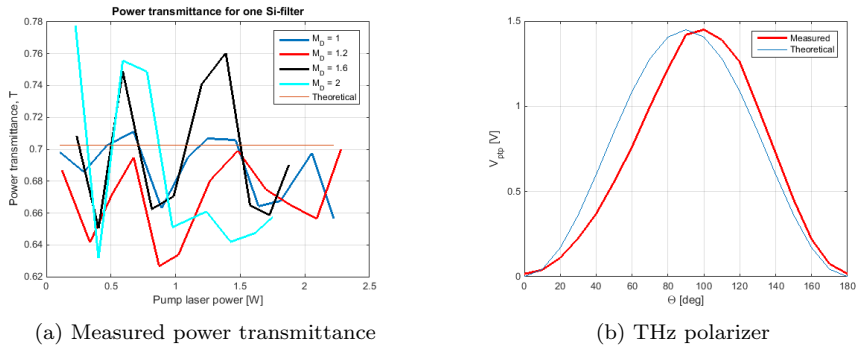


Figure 24: Measured power transmittance for Si-wafers at 1 THz and polarization of the emitted radiation.

### Imaging with THz camera

Imaging of the beam directly on the camera chip at some distances from the chip is shown in figure 25.

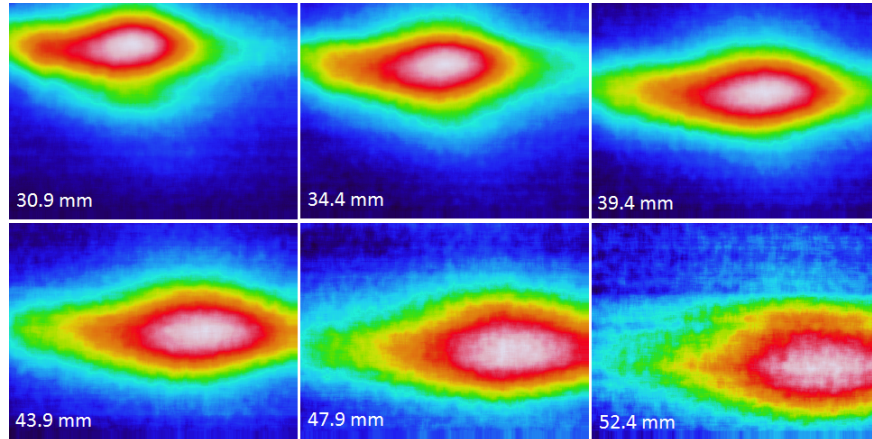


Figure 25: Beam profile at some distances from the THz camera chip. Note that the images is shown upside down because no lens is used.

The horizontal and vertical FWHM measurements of the profiles is shown in table 1.

Table 1: Vertical and horizontal FWHM values.

Chip distance [mm]	Horizontal FWHM [mm]	Vertical FWHM [mm]
30.9	4.55	1.67
34.4	4.95	1.79
39.4	5.42	1.76
43.9	6.2	2.11
47.9	>6.2	2.37
52.4	>6.2	2.63



Imaging of the THz source in the crystal done with the THz lens is shown in figure 26. Any notable changes in the profile could not be seen when different telescope designs were used. In figure 27 the horizontal and vertical profile of the source is shown.

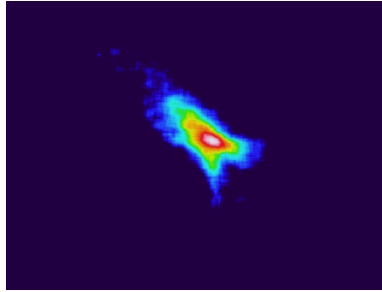


Figure 26: Image of the THz source in crystal.

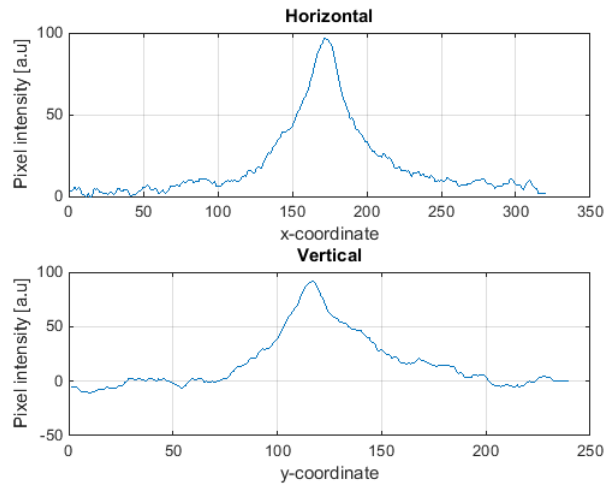


Figure 27: Profiles of the THz source in crystal.

By taking the FWHM values of the intensity profiles the size of the source can be determined to be 38 pixels horizontally and 42 pixels vertically corresponding to 1.49 mm and 1.65 mm respectively with this imaging system which can be seen as beam waists  $W_{0x} = 0.745\text{mm}$  and  $W_{0y} = 0.825\text{mm}$ .

## Intensity

If the source is approximated to be Gaussian then it is known that 99% of the power emitted is within 1.5 times the beam waist. Using the larger beam waist as radius and approximate the source as a circle the FWHM area of the source is then  $A = \pi \cdot W_{0y}^2 = 2.14 \cdot 10^{-6} \text{m}^2$ .

No time resolved detection was done so the peak pulse intensity cannot be determined. But for a pulse with a duration in the picosecond scale the peak intensity of a pulse close to the source would be in the order of:

$$I = \frac{P_{pulse}}{A} \sim \frac{0.4 \mu\text{J}/(10^{-12} \text{s})}{2.14 \cdot 10^{-6} \text{m}^2} \sim 10 \text{MW}/\text{cm}^2 \quad (25)$$

for  $0.4 \mu\text{J}$  THz pulse energy. Since the beam seems to have big divergence the intensity will decrease rapidly though.

## Divergence

Using the beam waists from the captured source and the measured beam profile values in table 1 the measured and theoretical divergence of the beam can be compared. The result is shown in figure 28.

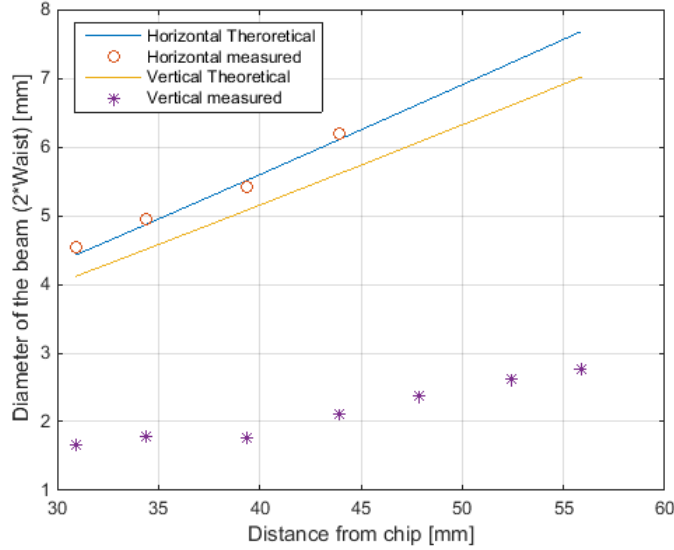


Figure 28: The theoretical and measured divergence of the beam profile using the imaged source. The last measurements in the horizontal direction is neglected since no FWHM value could be determined (see table 1). The theoretical values calculated at 1.9 THz

## 8 Discussion of results and conclusions

### 8.1 Detection and power

The first conclusion is that powerful THz radiation can be generated. The  $\lambda/2$ -plate before the crystal as well as the THz polarizer affects the measured power significantly. Since the optical frequencies are blocked with one or two Si-filters as well as the black filter on the detector the power most likely correspond to emitted THz radiation. Using the camera for detection confirms this since the radiation can be detected with the IR blocking filter mounted together with the Si-filters.

The other pyroelectric detector measured even a little bit higher power than the Microtech detector and this without any fine adjustments. Assuming that this power comes from pure THz radiation and the transmittance of the Si-filter is theoretical ( $T = 0.7$ ) the conversion efficiency can be up to  $\eta_{eff} = 0.87 \cdot 10^{-3}$  for this setup.

Even if the detectors shows emitted power in the mW-range it was hard to confirm this power with a non-pyroelectric detector since the other available detectors could not measure low power of few mW. This makes the results in figure 23 a little bit uncertain. Notable is also the fact that any power corresponding to higher frequencies than 3 THz cannot be measured by the Microtech detector. However since the wave mixing coherence length for frequencies above 2.3 THz is less than 1 mm as shown in figure 12 it can be assumed that most of the THz power is under 3 THz. The absorption of THz frequencies in LiNbO3 is also significantly higher for higher THz frequencies (see in section 4.2.4) which also gives the conclusion that most of the power is measured. It can also be stated that the conversion efficiency for this setup is in the order of  $\sim 1 \cdot 10^{-3}$  which is comparable with earlier research experiments on THz generation in LiNbO3 (Hoffmann and Fülöp [3]).

The spectral cut shown when the old lens  $L1$  was used, seen in figure 17 and figure 22, did not affect the measured power significantly. But one can think that it would affect the generation of higher THz frequencies because the generation comes from the difference frequencies in the spectrum, as well as the shape of the pulse entering the crystal making it less Gaussian-shaped.

The power transmittance by one Si-filter seen in figure 24 a) seems to agree on average around the theoretical for normal incident THz radiation. But since the filters just approximately was parallel to the plane of the crystal output surface some variations appeared.

### 8.2 Spatial profile

The profile of the source in the crystal was hard to capture with the camera using the THz lens. In figure 27 the source is captured with the camera plane parallel to the crystal output surface plane. However using the detector for power measurements showed that the highest power was measured when the detector was misaligned with the output surface at around 10 degrees, illustrated

in figure 29. Capturing the source with that alignment instead is shown in figure 30. A reasonable explanation why this misalignment shows higher power could be the big difference in refractive index for THz frequencies in the crystal compared to air. Using Snell's law and assuming the angle 10 degrees outside the crystal will give an angle of just 2 degrees misalignment inside the crystal at 1 THz which then can be estimated as an error of the tilt angle  $\gamma$  from the optimal tilt making the highest THz intensity going in this direction.

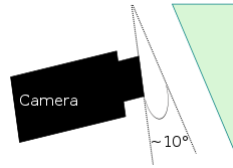


Figure 29: Camera alignment relative to the crystal.

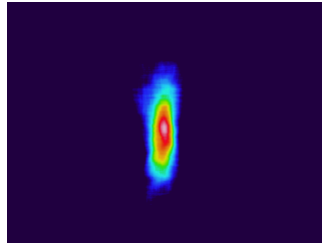


Figure 30: THz source.

The most interesting thing was however that none of the captured sources corresponded to the theoretical predictions of the beam profile. As seen in figure 28 the theoretical calculations using the captured beam waists  $W_{0x}$  and  $W_{0y}$  from the profile in figure 26 do not correspond at all in the vertical direction. In this figure the best theoretical fit of the measured and theoretical values could only be made for the horizontal beam divergence at the frequency of 1.9 THz. Why the vertical profile showing this behaviour is hard to explain.

Using the source captured in figure 30 was also hard to explain because the vertical FWHM value was larger for the source than the measured directly on the chip. This indicated that the beam instead of diverging was converging. A reasonable explanation of this behaviour can be that the THz beam could have curved wavefronts in the vertical direction making the beam converging to its vertical beam waist after the source.

The profiles captured without the THz lens can be seen as properly imaged though because the beam hit directly on the chip. In figure 25 and table 1 one can see that the beam diverges as the distance to the chip increases which is expected.

When capturing the profiles with the camera a higher SNR than maximum around 50 was hard to achieve even with a spatial filtering of  $N = 8 \times 8$  and

frame integration of  $n = 8$  because the camera software for some reason lagged. The lagging was always present independently of software settings but at higher values of frame integration it was almost impossible to save the data. At the initial phase of this project the camera software was tested on three different computers that all showed this behaviour. It seems though that a little bit less lagging is present using a computer with significantly better performance than the minimum requirements.

### 8.3 Polarization

As seen in figure 24 b) it can be concluded that the polarization of the emitted radiation is almost completely vertical but differs from the theoretical behaviour of the polarizer by  $10^\circ$ . This can depend on several things but it seems that it can depend on how the crystal was cut from the manufacturer. Neither the height of the laser beam entering the crystal or the polarizer alignment differed as much and could not give this polarization profile and a polarization misalignment from the laser would only give lower efficiency and not change the state of polarization. As for the rest the state of polarization was expected to be vertical and except the difference in 10 degrees the measured values fits nicely with the theoretical profile of a polarizer.

### 8.4 Telescope

The different telescope designs that were used seemed not to do any dramatic increase of the conversion efficiency but from figure 23 b) an overall better efficiency seemed to be best with a demagnification of  $M_D = 1.6$ . When the telescopes were used the alignment of the laser beam was slightly misaligned vertically at every telescope swap. The solution was simply to adjust mirror  $M3$  until the detector showed the highest amplitude on the oscilloscope and this was done initially when a new telescope was used. A mistake that made the measurements of the telescope a bit misleading was that introducing a telescope also introduced group velocity dispersion (GVD). In the optimization of this project a compensation of GVD was done by adjusting the amplifier which also should be done at each telescope swap.

## 9 Summation of the project

In this project it has been shown that intense short THz pulses can be generated with high efficiency using OR and the tilted pulse front technique, and that the setup can be designed to easily fit an optical breadboard  $60 \times 30 \text{ cm}^2$  to make it portable. It also shows that THz imaging can be quite challenging.

## 10 Appendix

### 10.1 Measuring power with Pyroelectric THz detector

The THz detector is based on pyroelectricity which basically can be explained as crystals that gives a voltage response to suddenly increased temperatures. This response can then be used to measure the power. The detector used in this project comes from Microtech instruments and have a detection range of 0.02-3 THz with a black filter mounted. By chopping the laser at certain chopping frequencies that correspond to different responsivities one can read the output voltage amplitude on an oscilloscope and convert it to power.

In this project the chopping frequency was set to 10 Hz. From the manufacturers data sheet<sup>2</sup> a responsivity-curve was attached showing the responsivity in V/W for a range of THz frequencies shown in figure 31.

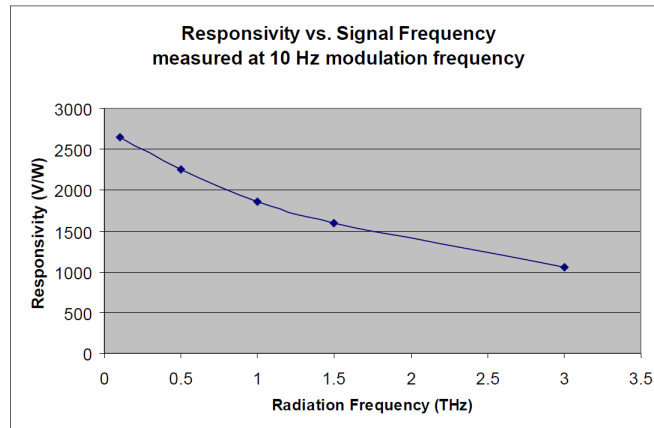


Figure 31: Responsivity at different THz frequencies.

The responsivity that was used to do the power calculations was 1800 V/W because the radiation emitted was assumed to be at the lower part of the measurable THz spectrum. Compared with measurements made with another pyroelectric detector showed even higher measured power than the Microtech detector which was a good indication that this responsivity was good.

If  $V_{ptp}$  is the peak-to-peak voltage amplitude and  $r$  the responsivity the power can be calculated by:

$$P = \frac{V_{ptp}}{r}$$

<sup>2</sup><http://www.mtinstruments.com/downloads/Pyroelectric%20Detector%20Datasheet.pdf>

## 10.2 Imaging with NEC THz camera

To image the THz source in the crystal the NEC THz camera can be used together with a THz lens and an IR blocking filter. The THz wave lens has a focal length of 28 mm and the IR blocking filter have transmittance greater than 80% for 1.5-7.5 THz and less than 0.1% transmittance for wavelengths 5-20  $\mu\text{m}$ . The camera chip have a pixel pitch of  $23.5\mu\text{m}$  and a resolution of  $320 \times 240$  pixels. Imaging of the THz source in the crystal can then be done as shown in figure 32.

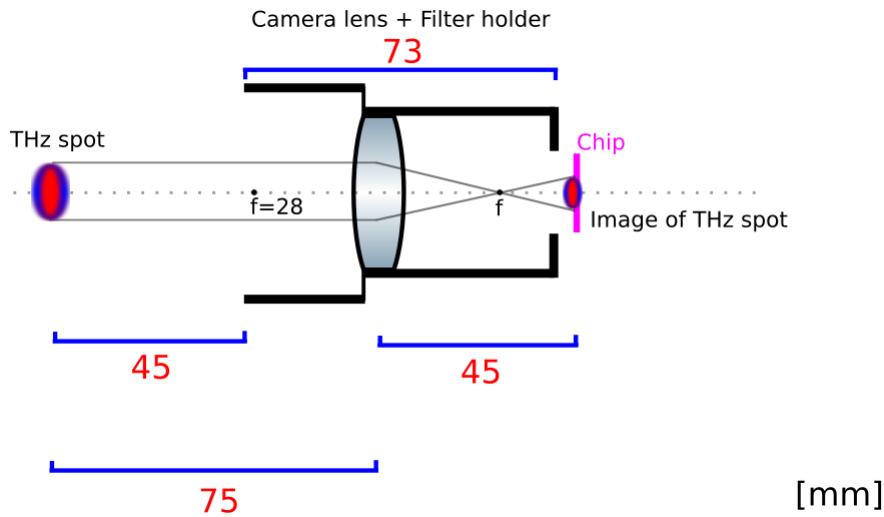


Figure 32: Imaging of the THz source with a THz camera.

In figure 32 the distances fulfill the imaging equation:

$$\frac{1}{f} = \frac{1}{d_1} + \frac{1}{d_2}$$

which will give a focused image of the spot on the camera chip. Since the image of the spot is magnified with a factor of 0.6 a measured distance on the image has to be divided by this factor when calculating the real spot size.

For example, if the diameter of a spot is 60 pixels then it corresponds to a real diameter of  $D = (60 \cdot 23.5\mu\text{m})/0.6 = 2.35\text{mm}$ .

### 10.2.1 Spatial filter and frame integration

To increase the signal to noise ratio (SNR) one can use spatial filtering and/or frame integration. In frame integration one can choose to integrate  $n = 1, 2, 4, \dots, 128$  frames which will be averaged in an optimal way and then displayed on the screen.

The spatial filtering will instead integrate and average the intensity of sub-areas corresponding to  $N \times N$  pixels in the original image for  $N = 1, 2, 3, 4, 6, 8, \dots, 24$ .

Note that depending on the wavelength and how detailed the image should be one have to think about the diffraction limit. The F-number using the NEC THz lens system is  $F_{\#} = 1$  and the pixel pitch is  $d_p = 23.5\mu\text{m}$  which gives that one can use a spatial  $N \times N$  filter where:

$$N \leq \frac{1.22\lambda}{d_p}$$

It can for example be calculated that since the transmittance of the IR filter is good for 1.5-7.5 THz the spatial filter can be set to  $N = 10$  in this region without loosing significant information.

For more details about the different methods read the appendix C of the NEC THz wave imager manual.



### 10.3 Sellmeier equation for LiNbO3

The extraordinary refractive index for LiNbO3 can approximately be calculated from the Sellmeier equation [5]:

$$n_e = \sqrt{2.3247 + \frac{2.2565\lambda^2}{\lambda^2 - 0.210^2} + \frac{14.503\lambda^2}{\lambda^2 - 25.915^2}} \approx 2.176, \lambda = 0.79\mu m$$

In figure 33 the extraordinary refractive index  $n_e$  is shown. The derivative  $dn_e/d\lambda$  is shown in figure 34.

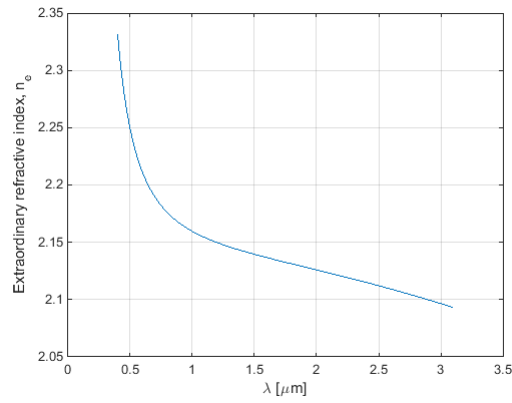


Figure 33: Extraordinary refractive index  $n_e$

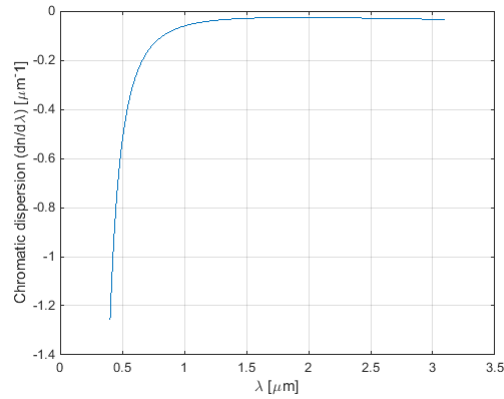


Figure 34: Derivative of  $n_e$

## 10.4 The Gaussian beam

The theoretical calculations of the THz profile was based on the theory of the Gaussian beam in *Fundamentals of photonics* [5].

For a beam with waist  $W_0$  the beam radius at the distance  $z$  can be calculated by:

$$W(z) = W_0 \sqrt{1 + \left(\frac{z}{z_0}\right)^2}$$

where  $z_0$  is the Rayleigh range:

$$z_0 = \frac{W_0^2 \pi}{\lambda}$$

The radius, i.e the divergence of the beam, depends on the wavelength.

## 10.5 Equipment used in the project

- Amplified Ti:Sapphire laser, repetition rate 4.25 kHz
- Optical breadboard, 60x30 cm<sup>2</sup>
- Plane-cylindrical convex lens  $f = 130\text{mm}$
- Plane-cylindrical convex lens  $f = 75\text{mm}$
- Two silver mirrors, size 1"
- Silver mirror, size 2"
- Two 800 nm  $\lambda/2$  plates
- Diffraction grating  $1800\text{mm}^{-1}$
- Si-wafers,  $R = 300\Omega/\text{cm}$ ,  $D = 50\text{ mm}$ , Thickness  $500\ \mu\text{m}$
- Mg-doped stoichiometric LiNbO<sub>3</sub> crystal. AR coated 800nm entrance surface, polished THz output surface.
- Pyroelectric THz detector, Microtech instruments
- Optical chopper, Thorlabs
- NEC THz wave imager camera (including IR blocking filter and THz wave lens)
- Wire grid THz polarizers, 1-3 THz range
- Cylindrical lenses for telescope,  $f = 300\text{mm}$ , 400 mm, -250mm, -150mm

## References

- [1] Yun-Shik Lee, "Principles of Terahertz Science and Technology", Springer Science+Business Media, LLC (2009), ISBN: 978-0-387-09539-4
- [2] Hai-Bo Liu, Hua Zhong, Nicholas Karpowicz, Yunqing Chen, Xi-Cheng Zhang, "Terahertz Spectroscopy and Imaging for Defense and Security Applications", Proceedings of the IEEE, Vol. 95, No. 8, August 2007
- [3] Matthias C Hoffmann, József András Fülöp, "Intense ultrashort terahertz pulses: generation and applications", 2011 J. Phys. D: Appl. Phys. 44 083001
- [4] János Hebling, Ka-Lo Yeh, Matthias C. Hoffmann, Balázs Bartal, Keith A. Nelson, "Generation of high-power terahertz pulses by tilted-pulse-front excitation and their application possibilities", J. Opt. Soc. Am. B/Vol. 25, No. 7/July 2008
- [5] Bahaa E. A. Saleh, Malvin Carl Teich, "Fundamentals of Photonics, second edition", John Wiley and Sons, Inc, 2007, ISBN: 978-0-471-35832-9
- [6] L. Pálfalvi, J. Hebling, J. Kuhl, Á. Péter, K. Polgár, "Temperature dependence of the absorption and refraction of Mg-doped congruent and stoichiometric LiNbO<sub>3</sub> in the THz range", Journal of Applied Physics 97, 123505 (2005); doi: 10.1063/1.1929859
- [7] J. A. Fülöp, L. Pálfalvi, G. Almási, J. Hebling, "Design of high-energy terahertz sources based on optical rectification", 7 June 2010, Vol. 18, No. 12, OPTICS EXPRESS
- [8] H. Hirori, K. Tanaka, "Nonlinear Optical Phenomena Induced by Intense Single-Cycle Terahertz Pulses", IEEE Journal of Selected Topics in Quantum Electronics (2013), 19(1)
- [9] H. Hirori, A. Doi, F. Blanchard, K. Tanaka, "Single-cycle terahertz pulses with amplitudes exceeding 1 MV/cm generated by optical rectification in LiNbO<sub>3</sub>", Applied Physics Letters 98, 091106 (2011); doi: 10.1063/1.3560062
- [10] C. M. Randall, R. D. Rawcliffe, "Refractive Indices of Germanium, Silicon, and Fused Quartz in the Far Infrared", Appl. Opt. 6, 1889-1895 (1967)
- [11] L. Arizmendi, "Photonic applications of lithium niobate crystals", phys. stat. sol. (a) 201, No. 2, 253–283 (2004) / DOI 10.1002/pssa.200303911

In some figures free vector graphics of optical components is used under creative commons license. Vector graphics created by Alexander Franzen (2006).  
<http://www.gwoptics.org/component.library/>